Vortex-lattice dynamics with channeled pinning potential landscapes

J. E. Villegas,[1] E. M. Gonzalez,[1] M. I. Montero,[2] Ivan K. Schuller,[2] and J. L. Vicent[1]

[1]*Departamento Física de Materiales, Facultad de Ciencias Físicas, Universidad Complutense de Madrid, 28040 Madrid, Spain*
[2]*Department of Physics, University of California, San Diego, La Jolla, California 92093-0319, USA*

We have studied vortex-lattice dynamics as a function of driving force direction, in superconducting Nb films with periodic pinning arrays of magnetic dots. Square and rectangular symmetry arrays define channels that guide the vortex-lattice motion. We investigated the effect of the driving force direction on the commensurability between the vortex-lattice and dots array. We also studied the transverse depinning of the vortex-lattice as is moving longitudinally along channels. We found that transverse depinning forces are enhanced with respect to the static situation. The results are discussed in terms of the dynamical evolution of order in the vortex-lattice.

PACS number(s): 74.78.Na, 74.25.Fy, 74.25.Qt

I. INTRODUCTION

The dynamics of the vortex-lattice (VL) in type-II superconducting films with periodic arrays of pinning centers have attracted increasing interest during the last years. Nanolithography techniques allow fabrication of ordered arrays of magnetic or nonmagnetic pinning centers whose shape, size, and position can be accurately controlled in the submicrometric range (for a review, see Ref. 1). This has allowed experimental exploration of many phenomena regarding static and dynamic properties of the VL. The most remarkable effects arising in this kind of nanostructured superconductors include commensurability between the VL and the periodic array of pinning centers,[2–12] competition between random and periodic pinning,[13] channeling effects in the VL dynamics,[14] or the ratchet effect.[15] Interestingly, much of the physics related to VL dynamics on periodic pinning potentials might apply to other systems in which transport of *small* particles takes place through fixed periodic potentials, as for instance colloids,[16] electrons in periodic antidot arrays,[17] etc. A worthwhile research area is how to guide the motion of such particles. The present paper is dedicated to study guided vortex motion on artificial pinning potentials under the action of an external driving force.

Earlier experimentally and theoretically VL dynamics on periodic pinning potentials, as a function of the direction of an applied driving force, seem to be in disagreement. Numerical simulations for square arrays of pinning centers[18,19] imply that, under appropriate conditions, vortex motion takes place only along preferred directions. For small driving forces, the vortex motion is guided along the main symmetry axis of the square array (sides and diagonals). Therefore the VL velocity is not parallel to the driving force when this is applied away from such privileged directions. This effect was explained in terms of commensurability between the VL and the periodic pinning potential which occurs only for motion along the sides or diagonals. Therefore,[18,19] the commensuration gives raise to transverse pinning, which keeps the VL moving along sides or diagonals even if the driving force is applied along other directions. Recent experiments in Pb thin films with square arrays of pinning centers have shown evidence for guided vortex motion along the sides of

the array.[20] However the mechanism responsible for this behavior seems to be different than the one discussed above,[18,19] since commensurability between the VL and the periodic array was observed for any direction of the driving force and of the VL motion.[20]

An essential ingredient of the origin of guided vortex motion arises from the VL dynamics on rectangular arrays of pinning centers. For these, theoretical calculations predict anisotropic VL dynamics, with easy-flow paths along the shortest lattice vector of the array.[21] This was experimentally shown for Nb thin films with rectangular arrays of magnetic pinning centers.[14] The physical origin of such easy-flow paths (channels) arises from the overlap of the pinning potential wells existing around each magnetic dot in the array. The smaller the distance between dots, the broader the pinning overlap, which produces channels for the VL motion along the direction of the shortest lattice vector of the array. Moreover, this channeling potential landscape efficiently locks in the motion of the VL along the easy-flow paths. Therefore, the VL is strongly guided along these privileged directions although the driving force is in another direction.[22]

In the present paper, we study in detail VL dynamics on channeled pinning potential landscapes. We compare the behavior of samples with square (fourfold symmetry) to those with rectangular (twofold symmetry) arrays of pinning centers. Using a special arrangement of electrodes we are able to measure the VL velocity as a function of direction of the applied driving force, for all in-plane directions. We show that the VL is guided along privileged directions in the case of twofold symmetries, while for the fourfold symmetry the VL moves following the direction of the driving force (Sec. III A). We have also performed experiments to study the effect of the applied driving force direction on the commensurability between the VL and the periodic array (Sec. III B). Finally, we explored transverse effects in the dynamics of the VL, which arise from the anisotropy in the pinning potential. In particular, we have investigated the VL depinning in the perpendicular direction to channels while driven longitudinally. When the VL is moving along channels at moderated velocity transverse depinning of the VL requires a larger force than in the static situation. This *transverse pinning*, together with the depinning mechanism itself, will be dis-
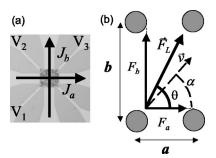
FIG. 1. (a) Micrograph of the measurement bridge. The array of magnetic dots is in the dark area over which the two currents J_a and J_b cross. (b) Sketch with notation definition of angles and directions with respect to the unit cell of the array.

cussed in terms of the dynamic evolution of commensurability, in Sec. III C.

II. EXPERIMENT

Ordered arrays of magnetic (Ni) dots were fabricated using e-beam lithography and sputtering techniques, on Si (100) substrates. The fabrication procedure has the usual steps; definition of the pattern by e-beam writing on the resist covering the substrate, developing, Ni sputter deposition and lift-off. After these, Ni nanostructures on top of the substrate are covered with a sputtered Nb thin film. Ni thickness (dots height) is 40 nm and Nb film is 100 nm thick. Further details on this procedure can be found elsewhere.[1] For this work, we have fabricated arrays with different anisotropies: sample A has an array with square symmetry, and lattice parameters $a \times b = 500 \times 500$ nm^2, while samples B and C have arrays with rectangular symmetry arrays, with lattice parameters $a \times b = 400 \times 500$ nm^2 and $a \times b = 400 \times 625$ nm^2, respectively. The dots diameter is $\phi = 225 \pm 20$ nm for all samples. Critical temperatures were $T_c = 8.21$ K for sample A, $T_c = 8.63$ K for sample B, and $T_c = 8.75$ K for sample C.

Magnetotransport experiments were carried out in a liquid He cryostat with a superconducting magnet and variable temperature insert control with 1 mK stability. The magnetic field was always perpendicular to the film plane and thus perpendicular to the injected dc electrical current J. The samples were patterned with a cross-shaped measuring bridge [see Fig. 1(a)], using optical lithography and ion-etching. This bridge allows injecting in the sample two crossing currents (J_a and J_b), and simultaneously measuring voltage drops along two perpendicular directions $V_a = V_3 - V_2$ and $V_b = V_2 - V_1$. With this arrangement, the direction and magnitude of the Lorentz force on the VL can be controlled: Since $\boldsymbol{F}_L = \boldsymbol{J} \times \boldsymbol{n} \phi_0$ (with $\phi_0 = 2.07 \times 10^{-15}$ Wb and $\boldsymbol{n}$ a unit vector parallel to the applied magnetic field), each one of the orthogonally injected currents yields the components $F_a = J_b \phi_0$ and $F_b = J_a \phi_0$, and therefore the magnitude of the Lorentz force is $F_L = \sqrt{F_a^2 + F_b^2}$, and its direction $\theta = \arctan(F_b/F_a) = \arctan(J_a/J_b)$ [see Fig. 1(b)]. Other forces acting on the VL, such as the Bardeen-Stephen viscous friction,[23] the Magnus force,[24] pinning, etc. are considered to be internal forces of the system. The only controllable ("driv-
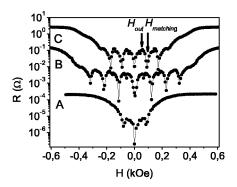
ing") external force is the applied Lorentz force. Our experiments address the dynamic response of the VL to this external force, as a function of its direction and magnitude. Since the electric field $\boldsymbol{E} = \boldsymbol{B} \times \boldsymbol{v}$, ($\boldsymbol{v}$ the VL velocity), the components of the VL velocity along a and b in the array are $v_a = V_b/(dB)$ and $v_b = V_a/(dB)$ (where d the distance between contacts), the magnitude $v = \sqrt{v_a^2 + v_b^2}$ and the direction $\alpha = \arctan(v_b/v_a)$. The definition of angles and directions with respect to the array of dots is depicted in Fig. 1(b).

The dc magnetoresistance in the mixed state of samples with periodic arrays of pinning centers exhibits well-known commensurability.[2–14] Deep minima develop as a consequence of the geometrical matching between the VL and the underlying periodic structure, which provides the pinning for the VL (see Fig. 2). For sample A minima occur when the applied magnetic field yields an integer number of vortices per unit cell of the array. Accordingly, the observed minima period is $\Delta H = 82$ Oe (see Fig. 2), in good agreement with the expected value $\Delta H = \phi_0/ab = 82.8$ Oe (with $a = b = 500$ nm). For the samples B and C, with rectangular arrays, two different regimes are found. In the low-field regime, the periodic minima correspond to an integer number of vortices per unit cell; for sample B, $\Delta H_{\mathrm{low}} = 104$ Oe ($\Delta H_{\mathrm{low}} = \phi_0/ab = 103$ Oe), while for sample C, $\Delta H_{\mathrm{low}} = 84$ Oe ($\Delta H_{\mathrm{low}} = \phi_0/ab = 82.9$ Oe). In the high-field regime, the period corresponds to matching between vortex-lattice parameter and the short side a of the rectangular array, $\Delta H_{\mathrm{high}} = 122$ Oe for sample B and $\Delta H_{\mathrm{high}} = 130$ Oe for sample C (in quite good agreement with $\Delta H_{\mathrm{high}} = \phi_0/a^2 = 129$ Oe). The transition between these two different regimes has been explained in terms of the reconfiguration in the vortex lattice from rectangular to square geometry.[12] Additionally, fractional matching effects[25] are present for sample B, for which shallow but clear minima appear at fields $0.5\Delta H_{\mathrm{low}} = 52$ Oe and $1.5\Delta H_{\mathrm{low}} = 156$ Oe.

III. RESULTS AND DISCUSSION

A. Anisotropic dynamics and guided vortex motion

As a first approach to VL dynamics, we measured the full vector $\boldsymbol{v}$ (VL velocity) for different directions (θ) but same

FIG. 2. Magnetoresistance for $\theta = 0^0$ for samples A ($T = 0.995T_c$, $J_a = 12.5$ kA cm^{-2}), B ($T = 0.99T_c$, $J_a = 12.5$ kA cm^{-2}), and C ($T = 0.99T_c$, $J_a = 12.5$ kA cm^{-2}). Curves have been shifted along the *y*-axis for clarity. The arrows indicate the magnetic fields H_{matching} and H_{out} (see text in Sec. II B).
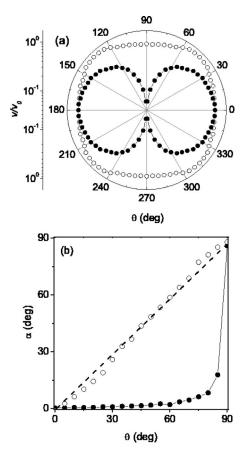
FIG. 3. (a) Vortex-lattice velocity $v=\sqrt{v_a^2+v_b^2}$ as a function of the direction θ of the driving force at the first matching field, normalized to velocity for $\theta=0$ (v_0). (b) Vortex lattice direction of motion $\alpha=\mathrm{arctag}(v_b/v_a)$ as a function of the direction of the driving force θ. Black circles are for sample C (rectangular array) at $T=0.99T_c$, $H=84$ Oe, and $F_L=1.03\times10^{-7}$ N m^{-1}. White circles are for sample A (square array) at $T=0.995T_c$, $H=82$ Oe, and $F_L=5.17\times10^{-7}$ N m^{-1}.

magnitude of the driving force F_L. Here we present only a brief description of the essential phenomenology for temperature $T\approx0.99T_c$ and applied magnetic fields corresponding to one vortex per pinning site in the array.

Figure 3(a) shows a polar plot of the magnitude v of the VL velocity as a function of driving force direction θ. The rectangular array (sample C, black circles) shows a very different behavior from the square array (sample A, open circles). For the rectangular symmetry, the VL dynamics is highly anisotropic, i.e., the VL velocity is strongly dependent on the direction of the driving force [Fig. 3(a)]. As the driving force is rotated closer to the long-axis (b) of the array, $\theta\rightarrow90°$, the VL velocity decreases by two orders of magnitude. For sample A (square array, open circles), VL velocity is slightly faster when the driving force is applied at $\theta=45°$ (or equivalents) than along any other direction, although the anisotropy is much lower than for the rectangular array. The VL velocity for a driving force along $\theta=0°$ or the equivalent directions is about 30% lower than for $\theta=45°$. Small imperfections existing in real samples, i.e., slightly different array lattice parameters or minor differences in the distance between contacts produce different velocities along $\theta=0°$ and

$\theta=90°$ and even different normal state electrical resistance. For instance, the resistance at $\theta=0°$ is around 7% higher than along $\theta=90°$.

Figure 3(b) shows the direction of motion of the vortex-lattice α plotted versus the direction θ of the driving force. For the rectangular array (sample C, black circles) the motion direction α is locked-in close to $\alpha=0$ although the driving force F_L is applied in a very different direction (up to $\theta=80°$). Above this angle the VL velocity rotates, but only at $\theta=90°$ it becomes parallel to the driving force ($\alpha\approx\theta$). This shows that for rectangular arrays (sample B shows similar behavior), the VL motion is strongly guided along the short array side a, due to the channeled pinning potential landscape.[22] On the contrary, for sample A (square array, white circles), the VL essentially follows the direction of the driving force ($\alpha\approx\theta$) in the whole angular range [see Fig. 3(b)]. This behavior is different to that theoretically predicted in numerical simulations,[18] and also differs from the experimental results for superconducting Pb samples with square arrays of antidots.[20] In both of these works, under some conditions, the vortex motion was guided along the principal symmetry axes of the square array. The difference between these earlier results and the one presented here may be due to the more intense pinning provided by magnetic dots as compared to antidots.[26] Stronger pinning, together with shorter inter-pinning sites distances in the array, yield easy-flow paths in the pinning potential that might be better defined than those of Ref. 20. The existence of such easy-flow paths (channels), that guide the VL along the shortest interdots distance in the rectangular arrays, has important implications. In the fourfold symmetry sample A there are *two* equivalent perpendicular directions along which interdots distances are the shortest, the two sides $a=b$ of the square array. Then two perpendicular and identical channels for the VL might be expected along such directions. Thus the VL can follow the driving force by switching from one channel to the other, moving in a staircase fashion instead of following straight trajectories. This kind of staircase motion has already been found in numerical simulations of similar systems, such as particles driven through colloidal lattices.[16] As shown above, the VL velocity is highest along the array diagonals. This is in qualitative agreement with the proposed staircase motion, which would yield a more disordered VL flow. In the following section we show that commensurability between the VL and the square array is degraded when the driving force is along the square diagonals, thus reducing pinning and yielding a higher VL velocity.

B. Dynamic and angular dependence of commensurability between the VL and the periodic array

To investigate the dependence of commensurability on the driving force direction, and VL velocity, we applied an approach proposed earlier.[13,22] We measured isothermal I-V characteristics close to T_c, in several applied magnetic fields and for several angles θ. From these I-V characteristics we calculate the VL velocity and direction of motion α for a given driving force F_L, obtaining $F_L(v)$ and $\alpha(v)$ as described in Sec. II. This is done in two different applied mag-
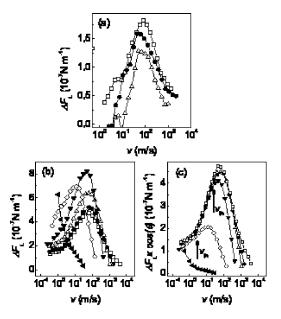
FIG. 4. (a) $\Delta F_L(v)$ at $T=0.99T_c$ for sample A, at the first matching field $H_{\text{matching}}=82$ Oe ($H_{\text{out}}=60$ Oe), for several $\theta=0°$ (squares), 30° (circles), 45° (up triangles). (b) $\Delta F_L(v)$ at $T=0.99T_c$ for sample C at the second matching field $H=168$ Oe ($H_{\text{out}}=140$ Oe), for several $\theta=0°$ (squares), 30° (circles), 45° (up triangles), 60° (down triangles), 75° (diamonds), and 85° (left triangles). (c) The same data from (b) but scaled as $\Delta F_L(v)\times\cos(\theta)$. v_{th} indicates the threshold velocity for $\Delta F_L(\theta)\times\cos(\theta)\approx\Delta F_L(\theta=0)$.

netic fields around the matching fields at which there are integer number of vortices per pinning site in the periodic array. In particular, a first curve is measured exactly at the matching field $F_{L\text{ matching}}(v)$, and a second one in a magnetic field below, in between matching fields $F_{L\text{ out}}(v)$ (see arrows in Fig. 2). The difference gives the pinning force enhancement at the matching field,

$$F_{L\text{ matching}}(v) - F_{L\text{ out}}(v) \equiv \Delta F_L(v). \qquad (1)$$

Figure 4(a) shows $\Delta F_L(v)$ for sample A (square array), for several directions θ of the driving force. For all angles $\Delta F_L(v)$ increases monotonically with the VL velocity, in good agreement with previous reports for similar samples.[13] This trend holds up to a maximum velocity, around $v \approx 100$ m/s, above which $\Delta F_L(v)$ decreases and tends to zero. The velocity at which $\Delta F_L(v)$ is maximum is independent of the direction θ of the applied driving force. However its magnitude decreases as the driving force is rotated from $\theta=0°$ to $\theta=45°$. Thus $\Delta F_L(v)$ for $\theta=45°$ is below all other curves.

The analysis for the second matching field $H=2\Delta H$ for the rectangular array sample C is depicted in Fig. 4(b). The results are in qualitative agreement with those for sample B, and are also similar to those around the first matching field.[22] $\Delta F_L(v)$ increases as the driving force approaches the long side of the array $b(\theta\rightarrow90°)$. The $\Delta F_L(v)$ maximum shifts from $v\approx100$ m/s to lower velocities above $\theta=60°$. This behavior can be understood by plotting $\Delta F_L(v)\times\cos(\theta)$ for

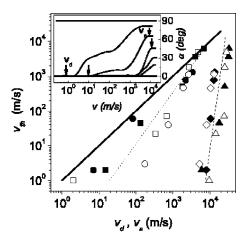FIG. 5. v_{th} versus v_d for sample C (black squares first matching field, black circles second matching field) and sample B (hollow squares first matching field, hollow circles second matching field); and v_{th} versus v_s for sample C (black triangles first matching field, black diamonds second matching field) and for sample B (hollow triangles first matching field, hollow diamonds second matching field). The continuous line is $v_{\text{th}}=v_d$ or $v_{\text{th}}=v_s$. Dashed and dotted lines are guides to the eye. Inset: vortex-lattice direction of motion $\alpha=\text{arctag}(v_b/v_a)$ versus its velocity $v=\sqrt{v_a^2+v_b^2}$ for several angles $\theta=0°$, 30°, 45°, 60°, 75°, 85°, and 90° (from bottom to top), for sample C at second matching field and $T=0.99T_c$. Arrows point to v_d and v_s.

each θ [Fig. 4(c)]. $\Delta F_L(\theta)\times\cos(\theta)\approx\Delta F_L(\theta=0)$ up to a given threshold velocity v_{th} [see arrows in Fig. 4(c)], which depends on the driving force direction, i.e., v_{th} decreases as $\theta\rightarrow90°$. This scaling behavior shows that, up to v_{th}, the component of the driving force F_b along the side b of the rectangular array has no effect on the VL dynamics, i.e., below v_{th} the driving force perpendicular to the channels plays no role.

To determine the VL motion direction (α) above and below the threshold velocity v_{th}, we calculate $\alpha(v)$ from the I-V characteristics at matching fields. An example is shown in the inset of Fig. 5. Each curve shows the VL motion direction α as a function of the velocity magnitude v, for several directions of the applied driving force θ. Three regimes are found for each curve (except for $\theta=0°$ or $\theta=90°$). In the first regime, the VL motion is guided along the channels in the pinning landscape (along the short axis of the array a, since $\alpha=0$). This regime holds up to a given velocity, v_d, at which the VL depins in the direction perpendicular to channels, i.e., at which the VL starts moving also along the long side of the array b ($\alpha\neq0$). In the second regime, α progressively rotates as VL velocity increases, and comes closer to θ. Finally, in the third regime above a given v_s, $\alpha\approx\theta$. Qualitatively, the same behavior is observed for samples B and C, at their first and second matching fields.

The relationship between v_{th}, v_d, and v_s in the three regimes above is shown in Fig 5, for both samples B and C, at their first and second matching fields. The correlations present in Fig. 5 are similar in both samples. The higher anisotropy of sample C (400×625 nm^2) compared to sample B (400×500 nm^2) results in slightly higher velocities v_{th}

and v_d. The most remarkable feature is that the threshold velocity v_{th} is always well below the velocity v_d at which the VL depins along the direction perpendicular to channels. This can be clearly seen in Fig. 5, since all the experimental points are well below the line $v_{th}=v_d$ or $v_{th}=v_s$.

The magnitude of $\Delta F_L(v)$ is a direct measure of the difference in interaction between the VL and the pinning potential at and out of matching field. $\Delta F_L(v)$ is positive when the pinning force at matching is enhanced with respect to the pinning force out of matching. This pinning enhancement is a consequence of the commensurability between the VL and the periodic array. $\Delta F_L(v)$ vanishes if the pinning force is similar at matching and out of it, indicating that the effect of the periodic pinning potential is reduced and there are no effects of commensurability between the VL and the periodic array. As explained in Ref. 13, the magnitude of $\Delta F_L(v)$ is proportional to the degree of ordering of the VL compared with the periodic pinning potential. Larger $\Delta F_L(v)$ values denote longer VL correlation lengths.[13] Thus $\Delta F_L(v)$ curves for different θ in principle monitor the dependence of the ordering of the VL on the direction of the driving force.

This suggests that for the rectangular array [Fig. 4(b)], at low velocities the ordering of the VL increases as the driving force is exerted closer to the long side b ($\theta \to 90°$). Contrary however, the scaling behavior displayed in Fig. 4(c) implies that $\Delta F_L(v)$ increases as $\theta \to 90°$ because the component of the driving force perpendicular to channels F_b is not effective below v_{th}. Therefore the increase of $\Delta F_L(v)$ as $\theta \to 90°$ [Fig. 4(b)] does not account here for a higher ordering of the VL, but it is simply due to the effective driving force being reduced to $F_a=F_L\times\cos(\theta)$. Aside from this, for each $\theta>0$, the decrease of $\Delta F_L(v)$ above v_{th} implies that the interaction between the VL and the pinning potential is reduced above this threshold velocity. As we shown in Fig. 5 $v_{th}<v_d$, i.e., when v_{th} is reached VL motion is still locked-in along channels. Therefore, the reduction of $\Delta F_L(v)$ above v_{th} is not related to the depinning of the VL in the direction perpendicular to channels, but to the value of F_b, the component of the driving force along such direction. This suggests that vortex dynamics in an anisotropic potential landscape cannot be understood within a simple model considering two orthogonal different pinning strengths and the vortex lattice moving in each direction independently, i.e., there are transverse effects that affect commensurability. Those are investigated in the following section.

As showed before, for the square symmetry array, $\Delta F_L(v)$ curves are qualitatively similar for all θ, but their magnitude decreases as the driving force changes from $\theta=0°$ to $\theta=45°$ [see Fig. 4(a)]. This indicates that the VL has a lower degree of ordering when it is pushed along the square diagonals ($\theta=45°$), since commensurability effects are reduced. This also agrees the results described in Sec. III A: for a given value of the driving force, the VL velocity is slightly higher when it is pushed along $\theta=45°$ than when it is pushed along other directions [see Fig. 3(a)].

The behavior for the square array might be related to the transverse effect described above. The square array might yield a pinning landscape with two perpendicular easy-flow channels for the VL. For instance, for $\theta=45°$ we propose that
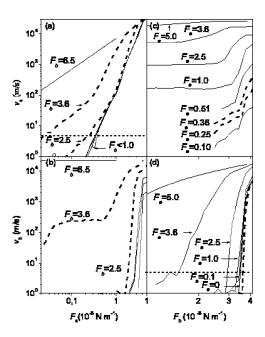

FIG. 6. For sample C at $T=0.99T_c$ and first matching field; (a) $v_a(F_b)$ and (b) $v_b(F_b)$ at several applied constants F_a (in 10^{-6} N m^{-1}). The horizontal dotted line is the velocity criteria at which $F_b=F_{cb}$. (c) $v_a(F_a)$ and (d) $v_b(F_a)$ at several applied constant F_b (in 10^{-6} N m^{-1}). The horizontal dotted line is the velocity at which $F_a=F_{ca}$.

the VL moves switching from one channel to the perpendicular one in a staircase fashion to follow the direction of the driving force. As the VL is moving longitudinally along the channels, there would be a component of the driving force perpendicular to the channel. As found for the rectangular arrays, the application of a transverse force affects the interaction between the VL and the pinning potential: commensurability effects are reduced [$\Delta F_L(v)$ decreases], ordering of the VL is lower, and therefore the pinning is weaker.

C. Transverse effects

To gain further insight into transverse effects, we have performed another set of experiments on samples B and C (samples with rectangular arrays). In these experiments we measure v vs F_L in one direction while a constant transverse force is applied. At the same time, we monitor the VL velocity along the transverse direction. These experiments were done both along and perpendicular to the direction of the channels in the potential landscape. In our notation, F_a and v_a are the force and velocity, respectively, along the channels, and F_b and v_b the force and perpendicular to the channels. The results for sample C at the first matching field (one vortex per pinning site) are shown in Fig. 6.

Figure 6(a) shows the velocities along the channels $v_a(F_a)$ for several applied transverse forces F_b. VL velocities in the direction perpendicular to channels v_b measured simultaneously are depicted in Fig. 6(b). For any transverse force $F_b<10^{-6}$ N m^{-1}, $v_a(F_a)$ curves are almost identical, i.e., dynamics along the channels is not affected by F_b. Above $F_b=2.5\times10^{-6}$ N m^{-1}, the $v_a(F_a)$ curve shifts to lower F_a, a

linear (Ohmic) regime develops at low driving forces F_a, and the depinning force along channels F_{ca} is reduced (critical depinning forces F_{ci} have been always taken as the force needed the cause $v_i > 5$ m/s. This occurs even if this transverse force is not high enough to depin the VL in the direction b perpendicular to the channels [Fig. 6(b)]. This in agreement with Sec. III B, where we found that above a given velocity for guided VL motion along channels, commensurability effects are degraded if a perpendicular driving force is present, even before depinning in the perpendicular direction takes place.

Figure 6(d) shows $v_b(F_b)$ along the perpendicular to channels, for several constant F_a applied along the channels. The velocity along the channels v_a is depicted in Fig. 6(c). For $F_a = 0$ or $F_a = 1.03 \times 10^{-7}$ [this yields $v_a \lesssim 20$ m/s, see Fig. 6(c)], $v_b(F_b)$ are very similar and also the critical forces F_{cb} are the same. However for 2.5×10^{-7} N m^{-1} $\leqslant F_a \leqslant 5.17 \times 10^{-7}$ N m^{-1}, $v_b(F_b)$ curves are shifted to higher F_b [dashed curves in Fig. 6(d)] and F_{cb} are enhanced. Within this range of forces F_a the VL flows along channels with velocities in the range $v_a \approx 20$–100 m/s before depining in the perpendicular direction takes place [see Fig. 6(c)]. That is to say, when the VL is moving along the channels at moderate velocities, the critical force F_{cb} is slightly higher than the static critical force observed for $v_a = 0$. However, as the force along the channels F_a is further increased and for longitudinal VL velocities $v_a > 100$ m/s ($F_a > 10^{-6}$ N m^{-1}), the critical force for depinning in the transverse direction F_{cb} drops monotonically. In summary, for a given range of velocities $v_a \approx 20$–100 m/s, the VL motion along the channels gives raise to transverse pinning yielding enhanced transverse critical forces.

Transverse pinning in driven lattices was theoretically predicted by Giamarchi and Le Doussal,[27,28] and observed in numerical simulations for many systems.[29–33] Barriers for transverse depinning may appear in longitudinally moving lattices if a dynamic mechanism enhances the transverse correlations of the lattice. In our system, VL correlations would be enhanced because of the interaction between the VL and the periodic pinning potential. As we showed in Sec. III B, commensurability effects are enhanced when the VL velocity increases, as the effect of intrinsic (disordered) pinning is overcome and the periodic one becomes dominant.[13] The parameter we used to monitor this evolution, $\Delta F_L(v)$, increased monotonically up to a maximum value at a VL velocity around 100 m/s. The enhancement of commensurability effects reflects a higher ordering of the VL, i.e., longer VL correlation lengths. In such regime, it is expected that the VL presents a higher degree of topological order along the transverse than along the longitudinal direction.[14,34] The enhanced transverse correlations for velocities 20 m/s $< v <$ 100 m/s would be responsible for the observed transverse pinning in our system. Recalling again the evolution of $\Delta F_L(v)$ (Sec. III B) the fact that transverse pinning disappears for $v_a \approx 100$ m/s can be also understood, since above that velocity commensurability effects progressively smear out. This explains the subsequent decrease of F_{cb} for velocities $v_a > 100$ m/s.

The behaviors discussed above for rectangular arrays are summarized in Fig. 7. Here similar data for sample B are
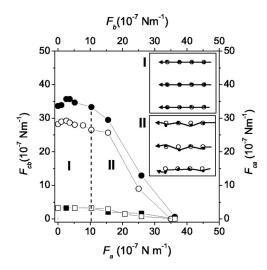

FIG. 7. Left-bottom axes: Critical depinning force F_{cb} as a function of the applied transverse force F_a, at first matching field for samples B (hollow circles) and C (black circles). Right-top axes: Critical depinning force F_{ca} as a function of the applied transverse force F_b at first matching field for samples B (hollow squares) and C (black squares). For an explanation on areas I and II, see text. The pictures represent vortex motion in regimes I and II, as explained in the text.

also included. In this graph, the critical depinning force as a function of the applied transverse force is depicted for both directions along (F_{ca}) and perpendicular (F_{cb}) to channels. The main difference in the results for samples B and C is that the higher anisotropy of sample C yields higher values of the critical depinning force F_{cb}.

The area of the plot is divided into two regions, I and II. The area labeled as I corresponds to low transverse driving forces (F_a or $F_b \leqslant 10^{-6}$ N m^{-1}). In this range depinning force along channels F_{ca} is not affected by F_b. However the depinning force in the direction perpendicular to channels F_{cb} is slightly enhanced. In this range F_a yields moderate v_a along the channels, which increases VL topological order and transverse correlations because of the optimum interaction with the periodic potential substrate (commensurability). Before depinning along b takes place [i.e., below the line $F_{cb}(F_a)$], ordered flow of the VL develops along the channels. A sketch of vortex motion is shown in the inset of Fig. 7.

In the region labeled II, for transverse forces 10^{-6} N m^{-1} $\leqslant F_a$, $F_b \leqslant 3.5 \times 10^{-6}$ N m^{-1}, the critical depinning forces F_{ca} and F_{cb} decrease as the corresponding transverse forces F_b or F_a are further increased. In this range F_a causes high VL velocities along the channels, reducing commensurability as we showed in Sec. III B, thus causing F_{cb} to decrease. F_b reduces the VL correlations in the direction perpendicular to channels, which weakens pinning and commensurability effects. Therefore F_{ca} also decreases with F_b in this regime. Above F_{ca} and with $F_b < F_{cb}$, the VL motion is guided along channels, but in a more disordered flow, as sketched in the inset of Fig. 7.

IV. CONCLUSIONS

We have investigated angular dependent dynamics of the VL in samples with ordered arrays of magnetic pinning cen-

ters. The whole in-plane angular range has been explored. Arrays of fourfold symmetry (square arrays) and twofold symmetry (rectangular array) have been studied. In summary the main results are:

(a) The magnetic character of the dots creates a very strong pinning potential around each dot in the array. Because of this, the overlap of pinning potential wells around contiguous magnetic dots yields easy-flow paths for the VL along the directions which has the shorter distance between dots. This gives raise to a "channeled" pinning potential landscape.

(b) In samples with square arrays the vortex dynamics shows fourfold symmetry and the VL mean motion direction is parallel to the driving force.

(c) In samples with arrays of rectangular symmetry, the VL motion has easy-flow paths (channels) along the direction of the shortest lattice vector of the array. Under some conditions the VL is strongly guided along those channels and because of this the VL velocity is away from the driving force direction.

(d) Commensurability effects between the VL and the array unit cell were studied applying forces perpendicular to the VL motion. Two transverse competing effects develop. When the VL is moving along channels and a strong enough perpendicular force is applied, ordering in the VL degrades and thus pinning forces related to commensurability decrease. On the other hand, motion along channels at moderate velocities enhances VL ordering and transverse correlations, yielding enhanced transverse pinning. Because of these effects, in the twofold symmetry potential landscapes, the magnitude of the components of the driving force along the two symmetry axes determine the different flow regimes of the VL: guided motion along channels with different degrees of ordering in the VL, or motion in the direction of the driving force.

[1] J. I. Martín, J. Nogués, K. Liu, J. L. Vicent, and I. K. Schuller, J. Magn. Magn. Mater. **256**, 449 (2003).

[2] O. Daldini, P. Martinoli, J. L. Olsen, and G. Berner, Phys. Rev. Lett. **32**, 218 (1974).

[3] A. T. Fiory, A. F. Hebard, and S. Somekh, Appl. Phys. Lett. **32**, 73 (1978).

[4] A. Pruymboom, P. H. Kes, E. van der Drift, and S. Radelaar, Phys. Rev. Lett. **60**, 1430 (1988).

[5] Y. Otani, B. Pannetier, J. P. Nozières, and D. Givord, J. Magn. Magn. Mater. **126**, 622 (1993).

[6] M. Baert, V. V. Metlushko, R. Jonckheere, V. V. Moshchalkov, and Y. Bruynseraede, Phys. Rev. Lett. **74**, 3269 (1995).

[7] J. I. Martín, M. Vélez, J. Nogués, and I. K. Schuller, Phys. Rev. Lett. **79**, 1929 (1997).

[8] Y. Jaccard, J. I. Martín, M.-C. Cyrille, M. Vélez, J. L. Vicent, and I. K. Schuller, Phys. Rev. B **58**, 8232 (1998).

[9] D. J. Morgan and J. B. Ketterson, Phys. Rev. Lett. **80**, 3614 (1998).

[10] V. Metlushko, U. Welp, G. W. Crabtree, R. Osgood, S. D. Bader, L. E. De Long, Z. Zhang, S. R. J. Brueck, B. Ilic, K. Chung, and P. J. Hesketh, Phys. Rev. B **60**, R12585 (1999).

[11] Y. Fasano, J. A. Herbsommer, F. de la Cruz, F. Pardo, P. L. Gammel, E. Bucher, and D. J. Bishop, Phys. Rev. B **60**, R15047 (1999).

[12] J. I. Martín, M. Vélez, A. Hoffmann, I. K. Schuller, and J. L. Vicent, Phys. Rev. Lett. **83**, 1022 (1999).

[13] M. Velez, D. Jaque, J. I. Martín, F. Guinea, and J. L. Vicent, Phys. Rev. B **65**, 094509 (2002).

[14] M. Velez, D. Jaque, J. I. Martín, M. I. Montero, I. K. Schuller, and J. L. Vicent, Phys. Rev. B **65**, 104511 (2002).

[15] J. E. Villegas, S. Savel'ev, F. Nori, E. M. Gonzalez, J. V. Anguita, R. Garcia, and J. L. Vicent, Science **302**, 1188 (2003); J. E. Villegas, E. M. Gonzalez, M. P. Gonzalez, J. V. Anguita, and J. L. Vicent, Phys. Rev. B **71**, 024519 (2005).

[16] C. Reichhardt and C. J. Olson Reichhardt, Phys. Rev. E **69**, 041405 (2004).

[17] J. Wiersig and K.-H. Ahn, Phys. Rev. Lett. **87**, 026803 (2001).

[18] C. C. de Souza Silva and G. Carneiro, Phys. Rev. B **66**, 054514 (2002).

[19] G. Carneiro, Phys. Rev. B **66**, 054523 (2002).

[20] A. V. Silhanek, L. Van Look, S. Raedts, R. Jonckheere, and V. V. Moshchalkov, Phys. Rev. B **68**, 214504 (2003).

[21] C. Reichhardt, G. T. Zimanyi, and N. Gronbech-Jensen, Phys. Rev. B **64**, 014501 (2001).

[22] J. E. Villegas, E. M. Gonzalez, M. I. Montero, I. K. Schuller, and J. L. Vicent, Phys. Rev. B **68**, 224504 (2003).

[23] J. Bardeen and M. J. Stephen, Phys. Rev. **140**, A1197 (1965).

[24] P. Noziéres and W. F. Vinen, Philos. Mag. **14**, 667 (1966).

[25] O. M. Stoll, M. I. Montero, J. Guimpel, J. J. Åkerman, and I. K. Schuller, Phys. Rev. B **65**, 104518 (2002).

[26] M. I. Montero, J. J. Akerman, A. Varilci, and I. K. Schuller, Europhys. Lett. **63**, 118 (2003).

[27] T. Giamarchi and P. Le Doussal, Phys. Rev. Lett. **76**, 3408 (1996).

[28] P. Le Doussal and T. Giamarchi, Phys. Rev. B **57**, 11356 (1998).

[29] K. Moon, R. T. Scalettar, and G. T. Zimanyi, Phys. Rev. Lett. **77**, 2778 (1996).

[30] S. Ryu, M. Hellerqvist, S. Doniach, A. Kapitulnik, and D. Stroud, Phys. Rev. Lett. **77**, 5114 (1996).

[31] C. Reichhardt and Franco Nori, Phys. Rev. Lett. **82**, 414 (1999).

[32] C. J. Olson and C. Reichhardt, Phys. Rev. B **61**, R3811 (2000).

[33] C. Reichhardt and C. J. Olson, Phys. Rev. B **65**, 094301 (2002).

[34] C. Reichhardt and G. T. Zimányi, Phys. Rev. B **61**, 14354 (2000).